Nonlinear formation of holographic images of obscurations in laser beams

C. Clay Widmayer, David Milam, and Simon P. deSzoeke

Computer models are used to simulate the nonlinear formation of images of obscurations in laser beams. The predictions of the model are found to be in good agreement with measurements conducted in the nonlinear regime corresponding to a typical solid-state laser operation. In this regime, peak-to-mean fluence ratios large enough to induce damage in optical components are observed. The amplitude of the images and their location along the propagation axis are accurately predicted by the simulations. This indicates that the model is a reliable design tool for specifying component staging and optical specifications to avoid optical damage by this mechanism. © 1997 Optical Society of America

Key words: Nonlinear optics, self-focusing, optical damage, fusion lasers.

1. Introduction

In high-peak-power lasers, such as the National Ignition Facility laser,[1] nonlinear effects can cause high-intensity images to be formed downstream from obscurations in the laser chain.[2,3] The peak fluences of these nonlinear images can reach levels high enough to damage expensive optical components. The susceptibility of a laser design to this damage mechanism can be reduced with accurate computer models that calculate the intensity and fluence of the beam at each component in the laser chain. Damage threats to the system can be identified by using such calculations, and the staging and quality of optical components can be adjusted to reduce the risk of damage that is due to image formation. We have modeled the formation of nonlinear images by obscurations resembling contamination or damage sites on optical components. These calculations have been compared with experimental measurements in which obscurations were placed in laser beams with nonlinear properties similar to those of our high-power solid-state lasers. The computer models are found to be in excellent agreement with the measurements, indicating that the models will serve as reliable tools for predicting the onset of nonlinear image formation in our designs.

The authors are with the Lawrence Livermore National Laboratory, 7000 East Avenue, L-465, Livermore, California 94550.

Received 30 April 1997; revised manuscript received 28 August 1997.

0003-6935/97/369342-06$10.00/0

The mechanism for nonlinear image formation is the creation of a type of Fresnel zone plate by nonlinear refraction.[4,5] The process is illustrated in Fig. 1. The diagram is schematic and does not represent an actual measured beam. In the figure, an intense beam propagates through two optical components. If a small scatterer, such as a speck of dirt or a small laser-induced damage site, is located on the first component, then illumination of the obscuration produces a scattered wave. The scattered wave interferes with the intense incident wave and produces an interference pattern or hologram.[6] For a small, round scatterer, like that shown in the figure, the interference produces a familiar bull's-eye pattern. The refractive index of the second nonlinear optic includes intensity-dependent terms. These terms impose the interference hologram onto the phase front of the incident beam. The nonlinear phase modulation refracts light from the main beam, creating a conjugate wave to the original scattered wave.[3] The conjugate wave converges to produce an intense holographic image of the scatterer downstream. Therefore, the second element acts like a Fresnel zone plate by focusing some of the incident wave to a bright image at intensities that may be many times larger than the initial primary wave. If a third optical component is located near one of these intense images, it may suffer laser-induced damage.

The amplitude of the converging wave and the beam's peak intensity near the conjugate image are determined by the nonlinear phase shift accumulated in the second element. The nonlinear phase shift, or B integral, is due to intensity-dependent

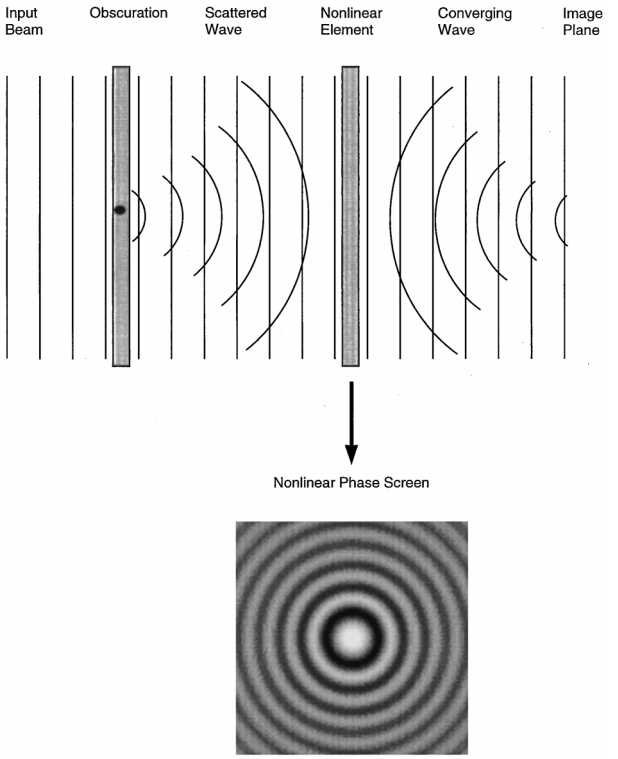

Fig. 1. Nonlinear image formation. An incident wave scatters from an obscuration and interferes with the main beam to produce an interference pattern. A phase screen is applied by the nonlinear (intensity-dependent) index of refraction of a second component downstream. The phase screen works like a Fresnel zone plate to focus light from the main beam on axis.

terms in the index of refraction, which can be written as

$$n = n_0 + \gamma I + \ldots . \tag{1}$$

Here n_0 is the unperturbed index, I is the intensity, and γ is the nonlinear coefficient. The B integral, measured in radians, is given by

$$B = \frac{2\pi}{\lambda} \gamma I t, \tag{2}$$

where λ is the vacuum wavelength of the laser light and t is the thickness of the nonlinear element. Perturbation models of nonlinear imaging[3] predict that the peak-to-mean intensity ratio is approximately proportional to B^2 in the plane of the image. The peak-to-mean modulation can be even higher in neighboring regions. Hence, very high intensities are predicted for the nonlinear image if B is allowed to assume large values. The damage threat posed by these images in fusion lasers is reduced by eliminating the high-spatial-frequency components of the images with spatial filters.[7,8]

To check the performance of the computer codes used to model this effect, we conducted a series of tests that recorded nonlinear images of obscurations similar to those found on optical components of solid-state laser systems. The tests were designed to clearly reveal the presence of the nonlinear images by reducing (as much as possible) other nonlinear effects. We achieved this by placing a 500-μm spherical obscuration in the path of the incident laser beam and allowing the beam to propagate through a 1-cm-thick sample of carbon disulfide (CS_2). CS_2 was chosen as the nonlinear medium for this experiment because its nonlinear coefficient, γ, is over 100 times greater than that of glasses typically used in solid-state lasers.[9–11] Large nonlinear phase shifts were then obtained in the CS_2 at modest intensities. The advantage of running the laser at reduced intensity is that the beam perturbations produced by nonlinear refraction in the components of the laser itself were minimized. So, the primary beam perturbation was that caused by the passage of the beam around the obscuration. The most profound difference between the experimental simulation and real systems is the distribution of the nonlinear phase pushback, B, in the optical medium. In actual systems, the B integral is distributed among several components whose thicknesses may be greater than that of the experimental sample considered here. Distributing the B integral through a bulk medium generally degrades the imaging effect because the interference hologram changes during the propagation through the medium. Fortunately, the threat of damage to optical components in real systems is reduced by this effect.

The results of our experiments were compared with numerical calculations. Similar comparisons have previously been reported that used one-dimensional geometries (a thin wire suspended in the beam).[12] The results reported here extend the analysis to include two-dimensional methods. Many real optical scatterers such as dirt or damage sites do not readily lend themselves to one-dimensional models. With B integrals equal to those seen in our systems, the 500-μm scatterer was found to produce nonlinear images with peak fluences up to ten times greater than the background beam. The computer simulations were found to be in good agreement with observed fluence distributions. This leads us to three conclusions. First, the computer models reliably predict the onset of nonlinear image formation and can be used to benchmark and evaluate hypothetical laser systems during the design phase. Second, high-nonlinear-index materials such as CS_2 are useful for generating large nonlinear effects at low power. This technique facilitates a comparison with modeling because measurements then clearly reveal nonlinear effects occurring in a single well-characterized subsystem. The measurements may be conducted at a reduced power whereby other nonlinear effects minimally influence the quality of the beam.

Finally, we have provided an independent confirmation that supports existing measurements of the nonlinear coefficient, γ, in CS_2. The most direct extant measurements of γ, using interferometry, were accurate to within 25%. We obtain a favorable agreement between our modeling and experiments by assuming a value of γ that is 7% below the interferometrically measured value.

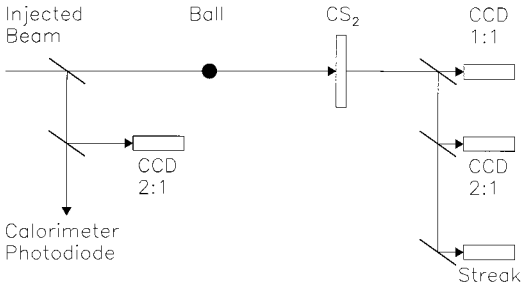

Fig. 2. Experimental arrangement for recording high-intensity images formed by nonlinear refraction.

2. Experimental Apparatus and Analysis

The experiments were conducted on the Optical Science Laser,[13] a 100-J Nd:glass laser. For the experimental tests, 1-ns quasi-Gaussian temporal pulses with mean fluences between 0.3 and 1.0 J/cm^2 were propagated. This range of fluences was chosen to produce phase pushbacks comparable with those seen between spatial filters on typical solid-state lasers. The spatial profile was nominally circular, with a diameter of 2 cm.

Figure 2 shows the experimental arrangement used for the self-focusing experiments. The beam was incident upon a 500-μm spherical ball suspended by thin, 12.5-μm-diameter diagonal wires. The beam then passed through a 1-cm cell of CS_2 sandwiched between two 1-cm-thick windows of fused silica located 94.3 cm downstream of the ball. The spatial profile of the beam was recorded by two charge-coupled device (CCD) cameras positioned to image a plane 86.7 cm behind the back surface of the cell. This plane was experimentally determined to be the location of a high-intensity image. The CCD cameras were Cohu 4810-series monochrome frame-transfer units, with the images acquired by BigSky framegrabbers. The framegrabbers were adjusted to indicate saturation at a signal level below the actual saturation signal of the camera. Linearity of the CCD signals was demonstrated by using the cameras as calorimeters. An image of the fluence distribution in a beam was recorded by one of the cameras, and the energy in the beam was measured with an absorbing glass calorimeter. The sum of the counts over the entire CCD image tracked the calorimetrically measured energy to within 2% for exposure levels up to the saturation level imposed by the framegrabber.

One CCD camera recorded a 1:1 image of the central 6-mm-diameter region of the beam containing the high-intensity image. The other produced a 2:1 demagnified image of the whole beam. A similarly demagnified image of the input beam was also obtained in a plane located upstream of the obscuration. Incident energy was measured with an absorbing glass calorimeter, and the temporal waveform of the pulse was recorded with a Hamamatsu diode, Tektronix SDC5000 oscilloscope and by a streak camera.

PROP92,[14,15] the computer code used for the calculations, employs a split-operator method[16] applied to the paraxial equation for beam propagation. Pure propagation proceeds by expanding the electric field in an angular spectrum of plane waves by the use of fast-Fourier-transform methods and multiplying each spectral component by an exponential propagator.[17] Nonlinear refraction was handled by applying an intensity-dependent phase in the near field, where gain and loss terms are also applied. The problem was solved in its entirety by a sequence of numerical steps alternating between pure propagation and refraction. The modeling is carried out in two spatial dimensions and one temporal dimension. As a way to initiate the calculation, the incident field was constructed from the measured beam profile at the plane of the scatterer. The field was represented on a two-dimensional grid transverse to the direction of propagation for a series of time intervals of varying lengths that spanned the duration of the temporal pulse. The individual time slices were then propagated independently and the resulting spatial intensity profiles were integrated numerically to produce a two-dimensional fluence distribution at the output. The model can thus imitate the integrative effects of laboratory diagnostic devices or provide time-resolved information of the temporal evolution of the pulse.

Some freedom exists in adjusting the input parameters of the model for comparisons with the experiment. For the simulations conducted here, a 1-cm^2 subregion of the beam was propagated by using a 512×512 calculational grid for a spatial resolution of 19.5 μm. This is comparable with the 23×27 μm pixel size of the CCD array. For validation of the choice of grid size, the model was compared with calculations conducted on a 1024×1024 grid, with which it was found to agree. Thirty-seven time slices were sufficient to fit the temporal shape of the pulse. The obscuration itself was treated as a perfectly absorbing 500-μm-diameter disk, with the edges smoothed to prevent a Gibbs phenomenon. If the edges are not smoothed, the absorbing obscuration produces a discontinuity in the field at the perimeter of the scatterer. A numerical artifact of the discontinuity is an overshoot, or ringing, when the field is Fourier transformed for propagation. Smoothing the edges prevents this discontinuity in the field. The CS_2 sample was modeled as ten contiguous slices, each with a thickness of 1 mm. We used a value of 3.0×10^{-5} cm^2/GW for the nonlinear coefficient, γ, of CS_2. This agrees with the direct interferometric measurement to within 7%.[9–11]

3. Results

Figure 3 shows a typical measured image of the central 6-mm-diameter region of the beam recorded 86.7 cm downstream from the CS_2 sample. The spatially averaged incident fluence for this shot was 0.603 ± 0.006 J/cm^2, and the nonlinear phase pushback through the sample was calculated from Eq. (2) to be 1.08 rad. The image of the obscuration is clearly visible in the center of the beam. Also visible are the

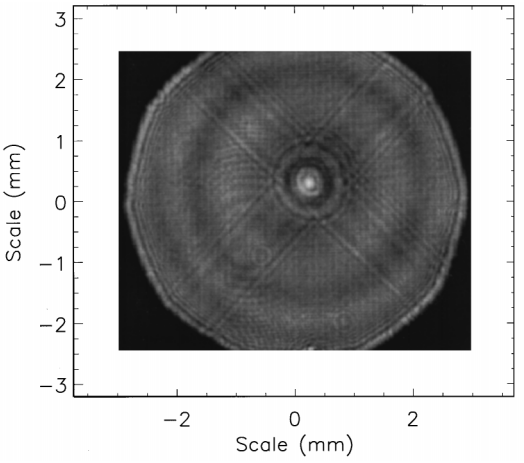

Fig. 3. CCD image of a high-intensity image formed by nonlinear refraction. The nonlinear phase pushback, B, for this shot is 1.08 rad.

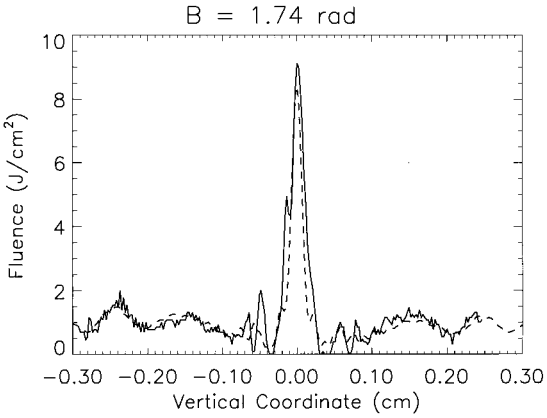

Fig. 5. Vertical line-outs through fluence distribution for calculated (dashed curve) and measured (solid curve) high-intensity images. The nonlinear phase pushback was 1.74 rad.

shallow diffraction ripples caused by the 12.5-μm-diameter suspending wires and the 6-mm aperture that preceded the CCD camera. The low-spatial-frequency ring structure surrounding the image is caused by diffraction around the scatterer and is independent of the incident beam pattern.

A comparison of the experimental data and the calculation is shown in Fig. 4. The solid curve is a vertical cut through the central peak of the measured fluence profile shown in Fig. 3. The dashed curve is a similar line-out from the computer simulation. The essential features of the experimental image are well reproduced by the simulation. A peak fluence of 2.51 J/cm^2 was predicted by the model, approximately 2% above the measured value of 2.44 ± 0.07 J/cm^2 and within the uncertainty of the measurement. The ratio of peak-to-mean fluence was measured to be approximately 4.2:1 from the experimental image.

The damage threat presented to optical components by the bright image is even higher than this suggests, however. The modulation that is due to the nonlinear image evolves during the pulse and is maximum when the B integral is highest. For a system with no saturating laser amplifiers, as is considered here, the maximum B integral occurs at the peak irradiance of the pulse. The experimental CCD image and the calculated fluence distribution generally underestimate the maximum peak-to-mean modulation because they are time integrated over the duration of the pulse. Although the experimental diagnostic (CCD array) does not give us time-resolved information of the evolution of the high-intensity image during the passage of the pulse, we can infer that information from the numerical simulation. For this shot, calculations predict an intensity of 3.39 GW/cm^2 at the peak of the temporal pulse, with a peak-to-mean intensity ratio of 5.8:1; this is 38% higher than that of the fluence distribution.

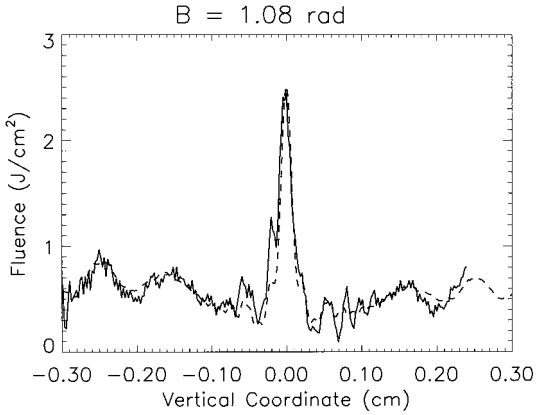

Fig. 4. Vertical line-outs through fluence distribution for calculated (dashed curve) and measured (solid curve) high-intensity images. The nonlinear phase pushback was 1.08 rad.

Good agreement between the simulation and experiment was obtained at all intensities studied in the test series. Figure 5 shows the experimental and calculated spatial profile line-outs for a shot with a B integral of 1.74 rad. This was the highest intensity shot in the series. The measured peak fluence of this shot was 9.1 ± 0.3 J/cm^2, and the peak-to-mean fluence ratio was 9.8:1.

The experimental measurement records the spatial profile of the beam in a single plane perpendicular to the propagation axis, but the computer simulation lets us infer the behavior of the beam along the entire propagation path. In Fig. 6 we show the peak amplitude of the nonlinear image as a function of propagation distance calculated for the shot shown in Figs. 3 and 4. The plane corresponding to the location of the CCD camera in the experiment is indicated. For this experiment, the CCD diagnostic imaged a plane where the peak fluence reached a local maximum, 86.7 cm downstream from the CS_2 sample. This plane was empirically determined to be a location of high-amplitude image formation. The calculation predicts the existence of a second plane experiencing bright fluence approximately 12 cm downstream from the first. The spatial profile of the beam at this location was not recorded during the

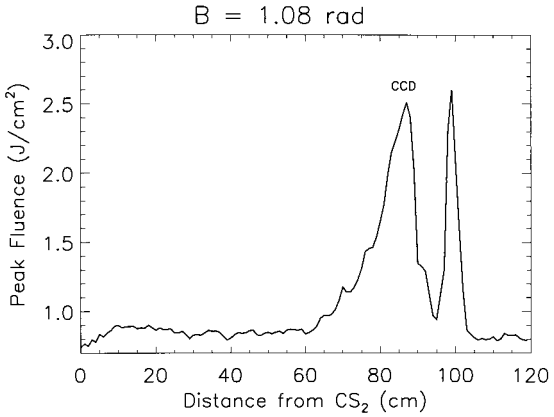

Fig. 6. Calculated variation of the peak fluence of a nonlinear image with propagation distance from the rear of the nonlinear sample. The location of CCD camera in the experimental measurement is indicated.

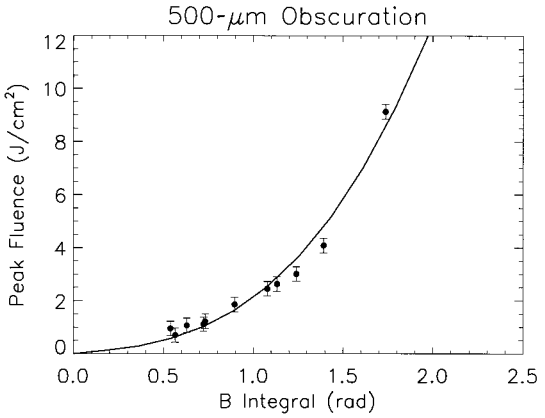

Fig. 8. Variation of the peak fluence of a nonlinear image with respect to the nonlinear phase pushback B. Points represent experimental data and the solid curve is the result of a numerical calculation.

experiment. Between these two planes the amplitude of the nonlinear image has a local minimum. The holographic image of the scatterer is produced with the most clarity at this location, which is known as the conjugate image plane. The conjugate plane is located 94–95 cm downstream from the back of the CS_2 cell, the same distance as from the scatterer to the front of the cell. Thus the nonlinear element is symmetrically located between the scatterer and its nonlinear image. The beam profile was not measured at the conjugate plane because the high-fluence regions on either side are of greater relevance to the issue of optical damage.

We identify the two peaks along the beam path in Fig. 6 with Fresnel diffraction near the conjugate image plane. The profile of the beam in the conjugate plane is shown in Fig. 7. At this location, the clarity of the image is greatest in the sense that the fluence over the 500-μm region mapping onto the obscuration is most uniform and the edges of the image are sharpest. Therefore, in the conjugate plane, the field near the center of the beam resembles a circle function of 500 μm in diameter. The fluence maxima are analogous to the single bright spot formed downstream when a flat beam illuminates a screen with a circular aperture. In Fig. 6, two peaks are present because there is a converging refracted wave upstream and a diverging wave downstream of the focal plane. For a scatterer of radius a, the bright peaks are located a distance a^2/λ on either side of the conjugate plane.

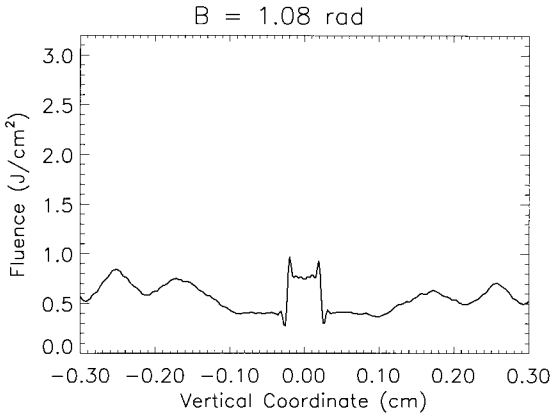

Fig. 7. Vertical line-out through the calculated fluence distribution of a high-intensity image in an image plane where object and image distances are equal.

Finally, we have examined the hot spot's dependence on input drive. Figure 8 shows the peak fluence of the image as a function of the nonlinear phase pushback B through the CS_2 sample. The solid curve represents nonlinear image amplitudes calculated by using a representative input spatial profile and pulse shape (that of the pulse shown in Figs. 3–6). In the calculation the mean input fluence was varied between 0.1 and 1.2 J/cm^2, giving a range of nonlinear phase pushbacks B between 0 and 2 rad. This is approximately the range of B integrals between spatial filters experienced on high-power solid-state lasers. The points are measured shot data taken with the image plane of the CCD camera fixed at a distance of 86.7 cm behind the CS_2 sample. The predictions of the computer simulations are in good agreement with the experiment for all values of B. For B integrals greater than 2 rad, the calculations predict nonlinear image amplitudes greater than 10 J/cm^2 and peak-to-average fluence ratios of greater than 10:1.

4. Summary

Using laser propagation codes in two spatial dimensions and one temporal dimension, we have simulated the formation of nonlinear images of obscurations by nonlinear refraction in lasers. A comparison with experimental data shows that we can accurately predict the shape, amplitude, and location of these nonlinear images. The results of the analysis indicate that circular obscurations of 500 μm in diameter are capable of producing images with amplitudes up to ten times greater than the mean

background fluence of the beam. These values are observed with nonlinear phase pushbacks comparable with those between spatial filters in high-power solid-state lasers. This indicates that the phenomenon may produce peak fluences that are damaging to expensive optical components even when the background beam is at a nominally safe value.

The success of the calculations ensures that the computer modeling will be a reliable tool for designing future lasers to avoid this dangerous phenomenon. The simulations are capable of identifying planes in the propagation path where high-amplitude image formation is liable to occur, alerting us to avoid locating vulnerable optical components there. With the computer codes we will also be able to investigate the effect of obscuration size on image formation. This will allow us to better estimate the damage threat in terms of the maximum allowable defect size. Because the quality of the optics directly determines their production cost, this information will allow us to better balance safety margin against damage with overall system cost.

The agreement between the experiment and modeling also confirms the usefulness of employing high-nonlinear-index materials, such as CS_2, to measure nonlinear phenomena experimentally. The technique is convenient when a quantitative comparison with a computer simulation is desired. The large nonlinear response of the experimental sample permits nonlinear effects to be observed at a relatively low power, where a high beam quality is more easily maintained. This also isolates the nonlinear influences on the beam to a single experimental sample whose properties can be well characterized, thus simplifying the model.

Finally, our results confirm previous measurements of the nonlinear coefficient γ of CS_2. Direct interferometric measurements have determined γ to within an uncertainty of $\pm 25\%$. In our study the most favorable agreement between the measurement and simulation occurred by using a value within 7% of the experimentally measured value.

The authors thank John Hunt, Ken Manes, and John Trenholme, who provided valuable input during the design of the experiment; Wade Williams and Paul Renard for guidance during the computer modeling; and Walter Sell who maintained and operated the Optical Science Laser facility during the experimental campaign. The PROP92 laser propagation code was originally developed at the Lawrence Livermore National Laboratory by Robert Nelson with advice and assistance from John Trenholme. The code was enhanced and modified by Richard Sacks, Scott Haney, and Mark Henesian. This research was performed under the auspices of the U.S. Department of Energy by the Lawrence Livermore National Laboratory under contract W-7405-ENG-48.

References

1. J. A. Paisner, E. M. Campbell, and W. J. Hogan, "The National Ignition Facility Project," Rep. UCRL-JC-117397 Rev. 1, June 1994 (Lawrence Livermore National Laboratory, Livermore, Calif.).
2. N. B. Baranova, N. E. Bykovskii, B. Ya. Zel'dovich, and Yu. V. Senatskii, "Diffraction and self-focusing during amplification of high-power light pulses," Sov. J. Quantum Electron. **4,** 1362–1366 (1975).
3. J. T. Hunt, K. R. Manes, and P. A. Renard, "Hot images from obscurations," Appl. Opt. **32,** 5973–5982 (1993).
4. V. I. Bespalov and V. I. Talanov, "Filamentary structure of light beams in nonlinear liquids," JETP Lett. **3,** 307–312 (1966).
5. J. B. Trenholme, "Theory of irregularity growth on laser beams," 1975 Laser Ann. Rep. UCRL-50021-75, 1975 (Lawrence Livermore National Laboratory, Livermore, Calif.).
6. D. Gabor, "A new microscope principle," Nature (London) **161,** 777–778 (1948).
7. J. T. Hunt, P. A. Renard, and W. W. Simmons, "Improved performance of fusion lasers using the imaging properties of multiple spatial filters," Appl. Opt. **16,** 779–782 (1977).
8. J. T. Hunt, J. A. Glaze, W. W. Simmons, and P. A. Renard, "Suppression of self-focusing through low-pass spatial filtering and relay imaging," Appl. Opt. **17,** 2053–2057 (1978).
9. K. J. Witte, M. Galanti, and R. Volk, "n_2-measurements at 1.32 μm of some organic compounds usable as solvents in a saturable absorber for an atomic iodine laser," Opt. Commun. **34,** 278–282 (1980).
10. W. E. Williams, M. J. Soileau, and E. W. Van Stryland, "Optical switching and n_2 measurements in CS_2," Opt. Commun. **50,** 256–260 (1984).
11. M. J. Moran, C. She, and R. L. Carman, "Interferometric measurements of the nonlinear refractive index coefficient relative to CS_2 in laser-system-related materials," IEEE J. Quantum Electron. **QE-11,** 259–263 (1975).
12. W. H. Williams, K. R. Manes, J. T. Hunt, P. A. Renard, D. Milam, and D. Eimerl, "Modeling of self-focusing experiments by beam propagation codes," ICF Quart. Rep. **6,** 7–14, UCRL-LR-105821-96-1, 1995 (Lawrence Livermore National Laboratory, Livermore, Calif.).
13. D. Eimerl, R. Boyd, and D. Milam, "The OSL: a new facility for laser research," ICF Quart. Rep. **1,** 108–113, UCRL-LR-105821-91-3, 1991 (Lawrence Livermore National Laboratory, Livermore, Calif.).
14. R. G. Nelson, "PROP92, a family of laser beam propagation codes," internal memorandum (unnumbered), 1992 (Lawrence Livermore National Laboratory, Livermore, Calif.).
15. R. A. Sacks, M. A. Henesian, S. W. Haney, and J. B. Trenholme, "The PROP92 Fourier beam propagation code," ICF Quart. Rep. **6,** 207–213, UCRL-105821-96-4, 1997 (Lawrence Livermore National Laboratory, Livermore, Calif.).
16. M. J. Feit, J. A. Fleck, and A. Steiger, "Solution of the Schrödinger equation by a spectral method," J. Comput. Phys. **47,** 412–433 (1982).
17. J. W. Goodman, *Introduction to Fourier Optics* (McGraw-Hill, San Francisco, 1968), pp. 48–54.